THE JOURNAL OF PHYSICAL CHEMISTRY C

pubs.acs.org/JPCC Article

Identification of Singlet Self-Trapped Excitons in a New Family of White-Light-Emitting Zero-Dimensional Compounds

Jun Xu,*,† Sai Li,† Chaochao Qin, Zongjing Feng, and Yaping Du*

Cite This: J. Phys. Chem. C 2020, 124, 11625−11630 Read Online

ACCESS | Metrics & More | Article Recommendations | Supporting Information

ABSTRACT: As illumination is a fundamental human need, the exploration of illumination sources possessing high efficiency and broadband white-light emission is highly desirable. Zero-dimensional (0D) metal halide compounds are promising candidates, and some lead-free antimony-containing compounds exhibit bimodal white-light emissions. However, their origins are still unclear. To solve this issue, we designed and prepared a new family of 0D metal halide compounds consisting of $[M(18\text{-crown-}6)]^+$ ($M = NH_4$, Rb) and SbX_5^{2-} (X = Cl, Br) units. We found that the emission profiles of 0D compounds are distinct to and well separated from that of 18-crown-6 ether, excluding the intraligand charge transfer mechanism proposed in several reports. Femtosecond transient absorption data and the compositional dependence of photophysical properties imply that bimodal white-light emission is induced by both singlet state and triplet state of the self-trapped excitons (^{1}STE and ^{3}STE) coupled to metal halides. These 0D compounds are also very efficient emitters, with a white-light photoluminescence quantum yield as high as 54%.

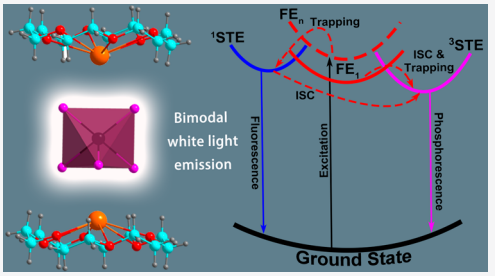

INTRODUCTION

Illumination is a fundamental human need and contributes up to approximately 20% of the global electricity consumption.[1] The advances in illumination sources from incandescent lamps to light-emitting diodes (LEDs) have saved considerable energy.[2,3] However, the light from commercial white LEDs is composed of narrow emissions from multiple components (e.g., red, green, and blue LED chips), not mimicking the broadband emission of natural sunlight.[3,4] In addition, such combined emitters suffer from other issues such as the increased cost, poor long-term color stability, significant efficiency loss due to self-absorption, etc.[5] The exploration of single-component white-light emitters possessing high efficiency and improved light quality is therefore of fundamental and practical importance.

Recently, organic−inorganic hybrid zero-dimensional (0D) metal halide compounds, consisting of individual polyhedrons or oligomers separated by bulky organic cations, have become promising candidates as single-component broadband white-light emitters.[6−12] The photoluminescence (PL) spectra of these 0D compounds are typically dominated by a broadband and highly Stokes-shifted emission owing to the phosphorescent transition between the triplet state of self-trapped excitons (^{3}STE) coupled to metal halides and their corresponding ground state. When both shape and position of the broadband emission profile are favorable, the white-light emission color can be observed.[7,8] Recently, bimodal white-light emissions have also been reported for several 0D compounds, especially the lead-free $SbCl_5^{2-}$-containing compounds.[9−12] The uniqueness of bimodal emission is that a second broadband emission appears in the short wavelength region with decreasing excitation wavelength, yielding a combined white-light emission along with the always existing broadband emission that is typical of 0D compounds. The bimodal white-light emission is therefore tunable, and its photoluminescence quantum yield (PLQY) can be higher than those of conventional 0D compounds.[12] However, the origin of the short wavelength emission remains unclear. Its PL lifetime (several nanoseconds) is in the typical range of a fluorescent process. Two mechanisms have thus been proposed: the intraligand charge transfer (ILCT),[9−11] or the fluorescent transition between the singlet state of self-trapped excitons (^{1}STE) coupled to metal halides and corresponding ground state.[12] In the former case, the fluorescence arises from the organic species, whereas it is associated with the metal halide polyhedrons for the second mechanism. However, even in the work with the proposed ^{1}STE mechanism,[12] the broadband emission of organic cations still covers the entire frequency region of the second emission and the ILCT mechanism cannot be ambiguously excluded. It is thus essential to examine whether the ^{1}STE mechanism is possible in 0D compounds.

To solve this issue, we have designed and synthesized a new family of organic−inorganic hybrid 0D compounds consisting

Received: March 19, 2020
Revised: April 22, 2020
Published: May 6, 2020

https://dx.doi.org/10.1021/acs.jpcc.0c02453
J. Phys. Chem. C 2020, 124, 11625−11630

of $[M(18\text{-crown-6})]^+$ (M = NH_4, Rb) and SbX_5^{2-} (X = Cl, Br). It is known that the weak and asymmetric PL peak of 18-crown-6 ether is at 424 nm, far away from the short wavelength emission (predicted to be at approximately 480 nm). By measuring the photophysical properties of these compounds, the origin of the unique bimodal white-light emission can be solved.

EXPERIMENTAL SECTION

Sample Preparation. Reagents: *N*,*N*′-Dimethylformamide (DMF, 99.8%) and acetone (HPLC grade) were purchased from Tianjin Bohai Chemical Reagent Co., Ltd. Rubidium chloride (RbCl, GR grade, 99.9%), antimony(III) trichloride ($SbCl_3$, 99.98% metal basis), and 18-crown-6 ($C_{12}H_{24}O_6$, 99%) were purchased from MackLin. Ammonium chloride (NH_4Cl, 99.5%) was purchased from Tianjin Fengchuan Chemical Reagent Technologies Co., Ltd. Ammonium bromide (NH_4Br, AR grade, 99%) was purchased from Aladdin. Antimony(III) tribromide ($SbBr_3$, 99.995% metal basis) was purchased from Alfa Aesar. All reagents and solvents were used without further purification.

Synthesis of $[(NH_4)(18\text{-crown-6})]_2SbCl_5$·DMF (compound **1**) single crystals: NH_4Cl, 18-crown-6, and $SbCl_3$ were mixed in a 2:2:1 molar ratio and dissolved in DMF, forming a clear solution. Large crystals were obtained by slowly diffusing acetone into DMF solution at room temperature overnight. White crystals were washed with acetone and dried under dynamic vacuum.

$[(NH_4)(18\text{-crown-6})]_2SbBr_5$·DMF (compound **2**) and $[Rb(18\text{-crown-6})]_2SbCl_5$·DMF (compound **3**) single crystals were synthesized similarly, but the precursors were replaced with NH_4Br and $SbBr_3$ for compound **2** and RbCl for compound **3**, respectively.

$[(NH_4)(18\text{-crown-6})]_2SbCl_{5-x}Br_x$·DMF single crystals were synthesized similarly using a mixture of NH_4Cl/NH_4Br and $SbCl_3/SbBr_3$. The exact x values were measured by ion chromatography analysis. The compounds were digested using an oxygen bomb, and the resulting products were absorbed using a sodium bicarbonate aqueous solution.

The bulk materials (microcrystals) of compounds **1**−**3** were synthesized using a rapid precipitation approach. For example, a concentrated DMF solution of NH_4Cl, 18-crown-6, and $SbCl_3$ in a 2:2:1 molar ratio was first prepared by stirring vigorously overnight. A large amount of acetone was then rapidly injected into the DMF solution. The white precipitates were collected, washed with acetone, and dried under dynamic vacuum.

The prototypical white-light-emitting diode (LED) device was fabricated by using a 310 nm LED chip (Shenzhen Lookinglong Technology Co., Ltd.) coated with compound **3**.

Single-Crystal XRD Measurements. Single-crystal XRD data were recorded on a Bruker D8 Venture diffractometer with a graphite monochromator at 150 K. Mo Kα radiation (λ = 0.71073 Å) and the ω-scan technique were used. The crystal structure was first solved with the ShelXL (Sheldrick, 2015) structure solution program using the Intrinsic Phasing solution method and Olex2 (Dolomanov et al., 2009) graphical interface. The raw structure was refined with version of ShelXL (Sheldrick, 2015) using the Least Squares minimization approach. The single-crystal structures have been deposited in the CCDC database (1988868, 1993135, 1993187).

Solid-State NMR Measurements. ^{13}C solid-state NMR (SSNMR) experiments were performed on a 400 MHz Bruker Avance III HB spectrometer with a ^{13}C Larmor frequency of 100.46 MHz, using a Bruker 4 mm $^1H/^{31}P-^{15}N$ CPMAS probe. The magic-angle spinning (MAS) rate was 10 kHz. The ^{13}C 90° pulse width (4.7 μs) was measured on adamantane, which was also used to calibrate the ^{13}C chemical shift by setting the downfield peak to 38.57 ppm relative to tetramethylsilane (TMS). The ^1H radiofrequency field for two-pulse-phase-modulated (TPPM) decoupling was 62.5 kHz. A 30° pulse of 1.56 μs and a recycle delay of 60 s were used.

Variable temperature ^2H static SSNMR experiments were performed on the same spectrometer and probe. The ^2H Larmor frequency was 61.44 MHz. A ^2H 90° pulse width of 6 μs was measured on D_2O, which was also used to calibrate the ^2H chemical shift by setting the peak to 4.80 ppm relative to TMS-d_{12}. The 90°-τ-90° spin echo sequence was used to record the accurate ^2H NMR line shapes. An interpulse delay (τ) of 25 μs and a recycle delay of 1 s were used. The sample temperature was regulated by a Bruker VT unit. The sample was kept at any given temperature for at least 10 min, ensuring thermal equilibrium before collecting the NMR signal.

PL Measurements. Room temperature PL emission and excitation spectra were recorded on an Edinburgh Instruments FLS1000 luminescence spectrometer. PLQY measurements were performed on the same spectrometer by means of an integrating sphere. The absolute error on the quantum yield values is about ±1%.

Temperature-dependent PL emission and excitation spectra were measured on an Edinburgh Instruments FLS 980 luminescence spectrometer, equipped with an OptistatDN variable liquid nitrogen cryostat (Oxford Instruments). Temperature control was achieved using an Omega CYC3200 autotuning temperature controller. Liquid nitrogen was used to cool the system.

Time-resolved PL emission data were collected at room temperature using an Edinburgh Instruments FLS980 spectrometer. The dynamics of emission decay were monitored with FLS980s time-correlated single-photon counting capability (1024 channels; 200 μs window) with data collection for 10 000 counts. Excitation was provided by an Edinburgh EPL-360 ps pulsed diode laser. The lifetime was obtained by exponential fitting.

The fs-TA measurements were carried out on a Helios pump−probe system (Ultrafast Systems LLC) coupled with an amplified femtosecond laser system (Coherent, 35 fs, 1 kHz, 800 nm). The probe pulses (from 350 to 600 nm) were generated by focusing a small portion (around 10 μJ) of the fundamental 800 nm laser pulses into a 1 mm CaF_2 crystal. The 320 and 365 nm pump pulses were generated from an optical parametric amplifier (TOPAS-800 fs).

UV−vis Diffuse Reflectance Measurements. Solid-state UV−vis diffuse reflectance spectra were measured on a Shimadzu UV-2600 UV−vis−NIR spectrometer using $BaSO_4$ powder as the reflectance reference. If the sample thickness and sample holder do not affect the reflectance, the absorption spectra can be calculated from the diffuse reflectance spectra by the Kubelka−Munk function: $F(R_\infty) = \alpha/S = (1 - R_\infty)^2/2R_\infty$, where R_∞ ($R_{sample}/R_{standard}$), α, and S are the coefficients for reflection, absorption, and scattering, respectively, assuming that the S is constant with respect to the wavelength. In the parabolic band structure, the band gap E_g and the absorption

https://dx.doi.org/10.1021/acs.jpcc.0c02453
J. Phys. Chem. C 2020, 124, 11625−11630

coefficient α of a direct band gap semiconductor are related through the equation $(\alpha\hbar\nu)^2 = C_1(\hbar\nu - E_g)$, where C_1 is a constant. Plotting the $(\alpha\hbar\nu)^2$ against $\hbar\nu$ (the Tauc plot) therefore yields the direct band gap of a powder sample.

RESULTS AND DISCUSSION

Single crystals of $[NH_4(18\text{-crown-}6)]_2SbCl_5\cdot DMF$ (compound **1**) were synthesized by diffusing the antisolvent (acetone) into a DMF solution of NH_4Cl, $SbCl_3$, and 18-crown-6 ether at ambient conditions. The single-crystal XRD (SCXRD) data reveal that it crystallizes in a monoclinic space group of *P*1. The complete crystallographic data are summarized in Table S1 (Supporting Information). As Figure 1a–c describes,

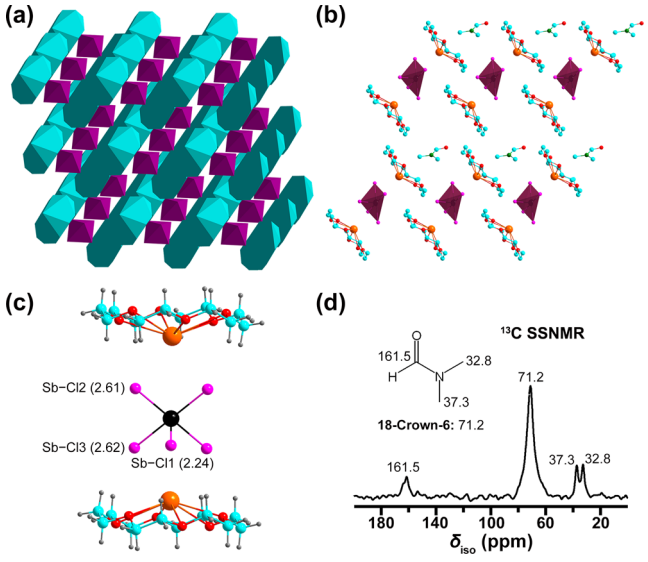

Figure 1. Schematic illustrations of $[NH_4(18\text{-crown-}6)]_2SbCl_5\cdot DMF$ (compound **1**) structure: (a) The structure viewed in three dimensions. $SbCl_5^{2-}$ and $[NH_4(18\text{-crown-}6)]^+$ ions are shown as dark purple and cyan polyhedrons, respectively. DMF molecules are omitted for clarity. (b) The structure viewed perpendicular to the (1, −2, 1) direction. $SbCl_5^{2-}$ ions are shown as dark purple polyhedrons, and hydrogen atoms are omitted for clarity. (c) The sandwich subunit with all Sb–Cl distances (in Å). Color code: H, gray; C, cyan; N, green; O, red; Cl, pink; NH_4, orange; Sb, black. (d) ^{13}C solid-state NMR (SSNMR) spectrum of the bulk materials of compound **1** synthesized using the rapid precipitation approach.

compound **1** belongs to a new type of 0D structure, with the $SbCl_5^{2-}$ pyramid sandwiched between two parallel $[NH_4(18\text{-crown-}6)]^+$ complexes. It is noted that the distance between two nearest neighboring $SbCl_5^{2-}$ pyramids is 10.3 Å, which is the longest among all antimony-containing 0D emitters.[10−14] DMF molecules are present in the voids, assisting to stabilize the 0D structure. The NH_4^+ ions are approximately 0.5 Å off the 18-crown-6 plane, likely due to the size mismatch.[15,16] The composition of compound **1** was further verified by thermogravimetric analysis (TGA, Figure S1) and X-ray photoelectron spectroscopy (XPS, Figure S2). The powder XRD pattern (Figure S3) reveals that compound **1** can be obtained in large quantities by using a rapid precipitation approach. As Figure 1d exhibits, the ^{13}C solid-state NMR (SSNMR) spectrum confirms the integrity of DMF and 18-crown-6 in bulk materials and there is no organic impurity.

It is generally believed that the efficient isolation between metal halides is the key for promising PL performances of 0D compounds.[13,14] Herein the bulky and quasi-planar $[NH_4(18\text{-crown-}6)]^+$ complex enables superefficient insulation between $SbCl_5^{2-}$ polyhedrons. As expected, an intense PL peak centered at 685 nm was observed at an excitation wavelength of 380 nm (Figure 2a), covering a broad frequency range that

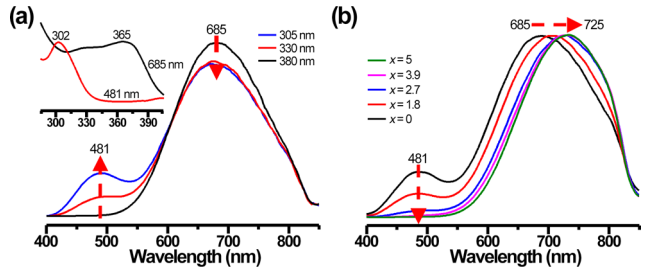

Figure 2. (a) Room temperature PL and PLE (inlet) spectra of compound **1** as a function of excitation or emission wavelengths, respectively. (b) PL spectra (λ_{ex} = 310 nm) of $[(NH_4)(18\text{-crown-}6)]_2SbCl_{5-x}Br_x\cdot DMF$ as a function of Br content *x*. Compound **1**: *x* = 0. Compound **2**: *x* = 5.

has extended to the near-infrared (IR) region. The PLQY is 57%. When shorter excitation wavelengths were used, a new broadband PL peak at 481 nm emerged, and its intensity grew with the decreasing excitation wavelengths, similar to that of several antimony-containing 0D compounds.[9−12] The bimodal emission of compound **1** yields tunable PL colors: the CIE chromaticity coordinates vary from (0.60, 0.39) to (0.46, 0.36) when the excitation wavelength decreases from 370 to 302 nm, corresponding to a transition of emission color from orange to "warm" white light (Figure S4). The high white-light PLQY (37%), high color rendering index (CRI: 76), and appropriate correlated color temperature (CCT: 2270 K) of compound **1** make it suitable for illumination.

The PL excitation (PLE) spectra of compound **1** indicate that the PL peak at 685 nm is associated with a broad excitation profile with the maximum at 365 nm, whereas the PL peak at 481 nm corresponds to a considerably narrower excitation peak centered at 302 nm. The two PL peaks thus must have different emission mechanisms. The characteristics of the PL peak at 685 nm are consistent with those of the previously reported ^{3}STE-induced emission in other $SbCl_5^{2-}$-containing 0D compounds:[9−12] broadband emission profile, high PLQYs, and large Stokes shifts. The peak position (685 nm) is also close to those of other compounds (583–648 nm).[9−12] However, the origin of the PL peak at 481 nm is unclear. As mentioned earlier, two emission mechanisms have been proposed in the literature, interpreted as the fluorescence from either ILCT[9−11] or ^{1}STE.[12] To the best of our knowledge, the ^{1}STE mechanism is still under debate.

PL lifetime decay curves of compound **1** were first measured at room temperature. The decay curves corresponding to both PL peaks can be simulated using a monoexponential decay function, with a PL lifetime of 3.8 μs for the 685 nm peak and 3.9 ns for the 481 nm peak (Figure S5), respectively. The slow decay of the 685 nm peak is consistent with a typical ^{3}STE-induced emission.[9−12] However, the 1000-fold reduction of PL lifetime of the 481 nm peak implies that it originates from a fluorescent process. Distinct from other $SbCl_5^{2-}$-containing 0D compounds with bimodal emissions, the fluorescence of the organic moiety (i.e., 18-crown-6) is very weak and asymmetric with the maximum at 424 nm,[17,18] inconsistent with the

https://dx.doi.org/10.1021/acs.jpcc.0c02453
J. Phys. Chem. C 2020, 124, 11625−11630

spectral features of the 481 nm peak. The 481 nm peak is thus unlikely an ILCT-induced emission. In addition, the PL lifetime is almost identical for large single crystals and microcrystals, and a linear relationship between the PL intensity and excitation power was observed (Figure S6), verifying that the emission is not due to the permanent defects.[19,20]

To further exclude the ILCT mechanism, we compared the PL spectrum of compound **1** with those of isostructural Br-substituted compounds $[(NH_4)(18\text{-crown-}6)]_2SbCl_{5-x}Br_x\cdot DMF$ (compound **2**: $x = 5$). If the 481 nm peak is due to ILCT, i.e., the fluorescence of organic moiety, the Br-substitution on metal halides should have negligible effects on this PL peak. However, as Figure 2b shows, the intensity of this PL peak drops dramatically with the incorporation of a heavy atom (Br) and eventually diminishes. The results confirm that the PL peak at 481 nm is associated with the metal halides, consistent with the ^{1}STE mechanism.

In 0D compounds, the excited electron−hole pair is stabilized by its strong coupling to a deformable metal halide polyhedron (i.e., the STE), and its formation can be probed by femtosecond transient absorption (fs-TA) measurements.[21,22] The fs-TA data of compound **1** was first collected but the corresponding photoinduced absorption (PIA) signals were noisy (Figure S7). In contrast, the PIA signals of isostructural $[Rb(18\text{-crown-}6)]_2SbCl_5\cdot DMF$ (compound **3**) were considerably stronger. With very similar photophysical properties (Figure S8), the fs-TA data of compound **3** are used to study the emission mechanism. As Figure 3a exhibits, the pump pulse at 320 nm induced a broadband excited state absorption plateau expanding the entire probe region, providing a direct evidence for the formation of STEs. Figure 3b shows that the rise time of the PIA band probed at 364 nm is within 0.3 ps,

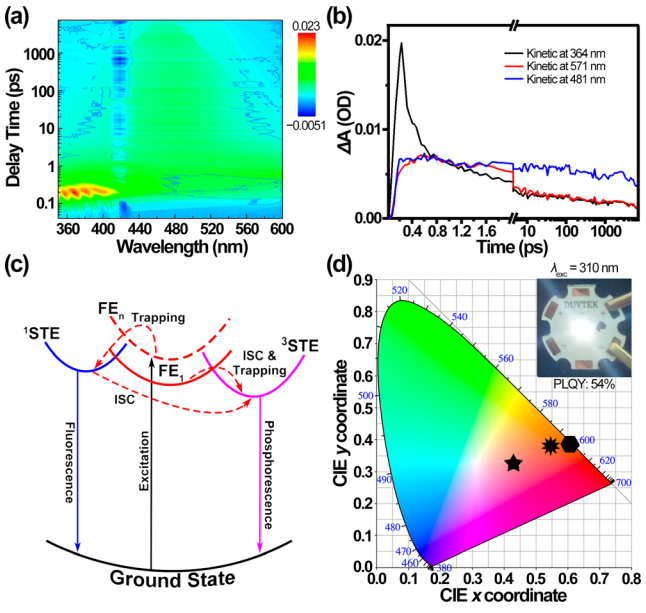

Figure 3. (a) Contour plot of femtosecond transient absorption (fs-TA) spectra of compound **3** as a function of wavelength and delay time (λ_{ex} = 320 nm) at room temperature. (b) Corresponding fs-TA kinetics probed at λ = 364, 481, and 571 nm. (c) Schematic diagram of the emission mechanism. (d) Corresponding CIE coordinates as a function of excitation wavelengths (star: 310 nm; flower: 340 nm; hexagon: 370 nm) and the image of a prototypical white LED device.

consistent with the formation of transient, photoinduced excited states. The intensity of this band decays rapidly after reaching the maximum, accompanied by the rise of the two PIA bands probed at 481 and 571 nm, respectively. The maxima of the two PIA bands were observed at 0.7 ps. The PIA band at 571 nm then decays slowly, whereas the decay of the PIA band at 481 nm is negligible even in several nanoseconds. The results therefore suggest that the PIA bands at 364, 571, and 481 nm are associated with the free exciton (FE), ^{1}STE, and ^{3}STE, respectively. The energy transfer processes were probed from FE to ^{1}STE/^{3}STE, and from ^{1}STE to ^{3}STE as well. The decrease of the short wavelength PL peak with increasing Br-substitution level is thus due to the enhanced intersystem crossing (ISC) efficiency (the so-called heavy-atom effect) between ^{1}STE and ^{3}STE.[23−25]

The mechanism of bimodal emission is therefore proposed as follows (Figure 3c): after photon absorption, the electrons are first promoted to excited states, forming FEs. The FEs can either be directly trapped in a short-lived ^{1}STE or be trapped later in a long-lived ^{3}STE after thermalization and ISC. The trapping in the ^{1}STE is followed by two processes, including a radiative recombination (i.e., the fluorescence) and the ISC to the ^{3}STE, while the trapping in the ^{3}STE is only followed by a radiative recombination (i.e., the phosphorescence).

In this work, we provide more exclusive evidence on the formation of ^{1}STE and corresponding energy transfer processes in 0D compounds. It is worth mentioning that the short wavelength PL peak present in several white-light-emitting 0D compounds, which were previously assigned to the ILCT-induced emission,[9−11] may also be due to ^{1}STE because of their similar characteristics. The unambiguous identification of ^{1}STE in 0D compounds has made significant progress in understanding the unique bimodal emission mechanism. These compounds are also efficient and stable emitting materials: the white-light PLQY of compound **3** is as high as 54%, and they are still very luminous after exposure to air for several months. As a proof of concept, a prototypical white LED device has been made by coating a commercial LED chip with compound **3** (Figure 3d). An intense white-light emission has been observed, with a CIE coordinate of (0.43, 0.34).

Distinct from the white-light emission solely from ^{3}STE, the bimodal white-light emission from ^{1}STE and ^{3}STE is tunable by modulating the ratio between ^{1}STE- and ^{3}STE-induced emissions and their efficiencies as a function of structural changes. The 0D compounds obtained in this work are not only ideal platforms to investigate the emission mechanism but also enable facile composition and property tunability. As Figures 2b and 4a−c and Tables S2−S5 describe, multiple photophysical properties such as the PL, PLE, absorption, and emission color vary monotonically with the composition of SbX_5^{2-} (X = Cl, Br). It is also noteworthy that the white-light PLQY can increase from 37% for compound **1** to 54% for compound **3** by simply replacing NH_4^+ with Rb^+. The lower PLQY of compound **1** can be rationalized by its higher nonradiative recombination. Even if short N···O distances (<3.10 Å) have been found in the crystal structure of compound **1**, the ^{2}H SSNMR data (Figure 4d) uncover that the strength of the N−H···O hydrogen bond is not sufficient to avoid the rapid reorientation of ND_4^+, which effectively averages the quadrupolar coupling interaction between ^{2}H and surrounding electric field gradient and results in a narrow

https://dx.doi.org/10.1021/acs.jpcc.0c02453
J. Phys. Chem. C 2020, 124, 11625−11630

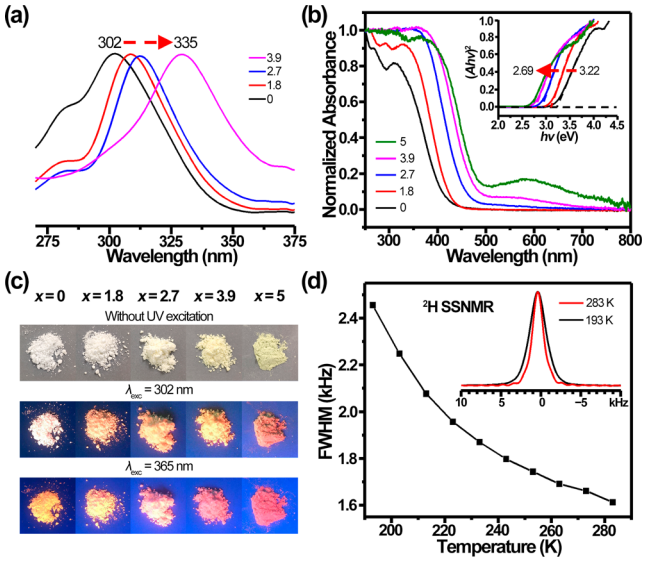

Figure 4. (a) PLE spectra of $[(NH_4)(18\text{-crown-}6)]_2SbCl_{5-x}Br_x\cdot DMF$ as a function of Br content x (λ_{em} = 685 nm). Compound **1**: x = 0. Compound **2**: x = 5. (b) Absorption (Kubelka–Munk transformed) spectra and corresponding Tauc plots as a function of x. (c) Corresponding PL images as a function of x. (d) Variable temperature ^{2}H SSNMR spectra (inlet) of the ND_4^+-labeled compound **1** and corresponding full width at half-maximum (fwhm) values.

and featureless ^{2}H NMR peak. The reorientation of ND_4^+ only slows (with a greater ^{2}H NMR peak width), and not stops even at 193 K.[26,27] More energy is thus exhausted during the breakage and reformation of hydrogen bonds, reducing the radiative recombination efficiency. The extensive exploration of this type of material, with exceptional compositional variability on both metal halides and organic–inorganic hybrid cations, can yield new materials with improved PL performances such as higher PLQY and CRI values, optimized CCT value and CIE coordinates, etc., exhibiting great potential in applications as white-light illumination sources.

CONCLUSIONS

The origins of bimodal white-light emissions present in several $SbCl_5^{2-}$-containing compounds are still not clear, especially the short wavelength emission peak. To verify if this peak is due to ILCT or ^{1}STE, we have designed and synthesized a new family of lead-free 0D compounds assembled with $[M(18\text{-crown-}6)]^+$ (M = NH_4, Rb) complexes and SbX_5^{2-} (X = Cl, Br). By measuring their photophysical properties, the ILCT mechanism can be excluded and the formation of ^{1}STE is verified by fs-TA experiments. We thus conclude that bimodal white-light emission is from both ^{1}STE and ^{3}STE coupled to metal halides. These compounds are also highly efficient white-light-emitting materials (PLQY can be as high as 54%), suitable for illumination applications such as white LEDs. The exceptional compositional variabilities on both metal halides and organic–inorganic hybrid cations enable further optimization of PL performance of this family of 0D compounds by varying the compositions.

ASSOCIATED CONTENT

Supporting Information

The Supporting Information is available free of charge at https://pubs.acs.org/doi/10.1021/acs.jpcc.0c02453.

Additional experimental details and data (PDF)

AUTHOR INFORMATION

Corresponding Authors

Jun Xu − *Center for Rare Earth and Inorganic Functional Materials, Tianjin Key Lab for Rare Earth Materials and Applications, School of Materials Science and Engineering & National Institute for Advanced Materials, Nankai University, Tianjin 300350, P.R. China;* orcid.org/0000-0003-3507-0159; Email: junxu@nankai.edu.cn

Yaping Du − *Center for Rare Earth and Inorganic Functional Materials, Tianjin Key Lab for Rare Earth Materials and Applications, School of Materials Science and Engineering & National Institute for Advanced Materials, Nankai University, Tianjin 300350, P.R. China*; Email: ypdu@nankai.edu.cn

Authors

Sai Li − *Center for Rare Earth and Inorganic Functional Materials, Tianjin Key Lab for Rare Earth Materials and Applications, School of Materials Science and Engineering & National Institute for Advanced Materials, Nankai University, Tianjin 300350, P.R. China*

Chaochao Qin − *Henan Key Laboratory of Infrared Materials & Spectrum Measures and Applications, Henan Normal University, Xinxiang 453007, P.R. China*

Zongjing Feng − *Center for Rare Earth and Inorganic Functional Materials, Tianjin Key Lab for Rare Earth Materials and Applications, School of Materials Science and Engineering & National Institute for Advanced Materials, Nankai University, Tianjin 300350, P.R. China*

Complete contact information is available at: https://pubs.acs.org/10.1021/acs.jpcc.0c02453

Author Contributions

†J.X. and S.L. contributed equally to this work.

Notes

The authors declare no competing financial interest.

ACKNOWLEDGMENTS

J.X. appreciates the financial support from the National Natural Science Foundation of China (project 21904071) and the Open Funds (KF1818) of the State Key Laboratory of Fine Chemicals. C.Q. acknowledges the financial support from the National Natural Science Foundation of China (project 11804084). Y.D. acknowledges the financial support from the National Natural Science Foundation of China (projects 21522106 and 21971117), 111 project (B18030) from China, the Open Funds (RERU2019001) of the State Key Laboratory of Rare Earth Resource Utilization, and the Functional Research Funds for the Central Universities, Nankai University (ZB19500202).

REFERENCES

(1) Bergh, A.; Craford, G.; Duggal, A.; Haitz, R. The Promise and Challenge of Solid-State Lighting. *Phys. Today* **2001**, *54*, 42–47.

(2) Uchida, Y.; Taguchi, T. Lighting Theory and Luminous Characteristics of White Light-Emitting Diodes. *Opt. Eng.* **2005**, *44*, 124003.

(3) Taguchi, T. Present Status of White LED Lighting Technologies in Japan. *J. Light Visual Environ.* **2003**, *27*, 131–139.

(4) Li, Y.; Rizzo, A.; Cingolani, R.; Gigli, G. Bright White-Light-Emitting Device from Ternary Nanocrystal Composites. *Adv. Mater.* **2006**, *18*, 2545–2548.

(5) Ye, S.; Xiao, F.; Pan, Y. X.; Ma, Y. Y.; Zhang, Q. Y. Phosphors in Phosphor-Converted White Light-Emitting Diodes: Recent Advances in Materials, Techniques and Properties. *Mater. Sci. Eng., R* **2010**, *71*, 1−34.
(6) Zhou, C.; Lin, H.; He, Q.; Xu, L.; Worku, M.; Chaaban, M.; Lee, S.; Shi, X.; Du, M.-H.; Ma, B. Low Dimensional Metal Halide Perovskites and Hybrids. *Mater. Sci. Eng., R* **2019**, *137*, 38−65.
(7) Roccanova, R.; Houck, M.; Yangui, A.; Han, D.; Shi, H.; Wu, Y.; Glatzhofer, D. T.; Powell, D. R.; Chen, S.; Fourati, H.; et al. Broadband Emission in Hybrid Organic−Inorganic Halides of Group 12 Metals. *ACS Omega* **2018**, *3*, 18791−18802.
(8) Yangui, A.; Roccanova, R.; McWhorter, T. M.; Wu, Y.; Du, M.-H.; Saparov, B. Hybrid Organic−Inorganic Halides $(C_5H_7N_2)_2MBr_4$ (M = Hg, Zn) with High Color Rendering Index and High-Efficiency White-Light Emission. *Chem. Mater.* **2019**, *31*, 2983−2991.
(9) Wang, S.; Li, L.; Sun, Z.; Ji, C.; Liu, S.; Wu, Z.; Zhao, S.; Zeb, A.; Hong, M.; Luo, J. A Semi-Conductive Organic−Inorganic Hybrid Emits Pure White Light with an Ultrahigh Color Rendering Index. *J. Mater. Chem. C* **2017**, *5*, 4731−4735.
(10) Wang, Z.-P.; Wang, J.-Y.; Li, J.-R.; Feng, M.-L.; Zou, G.-D.; Huang, X.-Y. $[Bmim]_2SbCl_5$: A Main Group Metal-Containing Ionic Liquid Exhibiting Tunable Photoluminescence and White-Light Emission. *Chem. Commun.* **2015**, *51*, 3094−3097.
(11) Wang, Z.; Zhang, Z.; Tao, L.; Shen, N.; Hu, B.; Gong, L.; Li, J.; Chen, X.; Huang, X. Hybrid Chloroantimonates(III): Thermally Induced Triple-Mode Reversible Luminescent Switching and Laser-Printable Rewritable Luminescent Paper. *Angew. Chem., Int. Ed.* **2019**, *58*, 9974−9978.
(12) Li, Z.; Li, Y.; Liang, P.; Zhou, T.; Wang, L.; Xie, R.-J. Dual-Band Luminescent Lead-Free Antimony Chloride Halides with Near-Unity Photoluminescence Quantum Efficiency. *Chem. Mater.* **2019**, *31*, 9363−9371.
(13) Zhou, C.; Lin, H.; Tian, Y.; Yuan, Z.; Clark, R.; Chen, B.; van de Burgt, L. J.; Wang, J. C.; Zhou, Y.; Hanson, K.; et al. Luminescent Zero-Dimensional Organic Metal Halide Hybrids with Near-Unity Quantum Efficiency. *Chem. Sci.* **2018**, *9*, 586−593.
(14) Zhou, C.; Worku, M.; Neu, J.; Lin, H.; Tian, Y.; Lee, S.; Zhou, Y.; Han, D.; Chen, S.; Hao, A.; et al. Facile Preparation of Light Emitting Organic Metal Halide Crystals with Near-Unity Quantum Efficiency. *Chem. Mater.* **2018**, *30*, 2374−2378.
(15) Steed, J. W. First- and Second-Sphere Coordination Chemistry of Alkali Metal Crown Ether Complexes. *Coord. Chem. Rev.* **2001**, *215*, 171−221.
(16) Ponomarova, V. V.; Rusanova, J. A.; Rusanov, E. B.; Domasevitch, K. V. Unusual Centrosymmetric Structure of $[M(18\text{-Crown-6})]^+$ (M = Rb, Cs and NH_4) Complexes Stabilized in an Environment of Hexachloridoantimonate(V) Anions. *Acta Crystallogr., Sect. C: Struct. Chem.* **2015**, *71*, 867−872.
(17) Jian, Y. F.; Fu, B.; Fu, S.; Liu, X. Synthesis, Crystal Structure, and Photoluminescence of a Lithium Perchlorate Complex with 18-Crown-6. *J. Struct. Chem.* **2019**, *60*, 1119−1125.
(18) Fu, S.; Fu, B.; Zhao, Z.; Liu, X. Synthesis, Crystal Structure, and Photoluminescence of a Lithium Isothiocyanate Compound with 18-Crown-6. *Z. Naturforsch., B: J. Chem. Sci.* **2018**, *73*, 85−89.
(19) Dohner, E. R.; Hoke, E. T.; Karunadasa, H. I. Self-Assembly of Broadband White-Light Emitters. *J. Am. Chem. Soc.* **2014**, *136*, 1718−1721.
(20) Benin, B. M.; Dirin, D. N.; Morad, V.; Wörle, M.; Yakunin, S.; Rainò, G.; Nazarenko, O.; Fischer, M.; Infante, I.; Kovalenko, M. V. Highly Emissive Self-Trapped Excitons in Fully Inorganic Zero-Dimensional Tin Halides. *Angew. Chem., Int. Ed.* **2018**, *57*, 11329−11333.
(21) Zhou, L.; Liao, J.-F.; Huang, Z.-G.; Wei, J.-H.; Wang, X.-D.; Chen, H.-Y.; Kuang, D.-B. Intrinsic Self-Trapped Emission in 0D Lead-Free $(C_4H_{14}N_2)_2In_2Br_{10}$ Single Crystal. *Angew. Chem., Int. Ed.* **2019**, *58*, 15435−15440.
(22) Yang, B.; Han, K. Charge-Carrier Dynamics of Lead-Free Halide Perovskite Nanocrystals. *Acc. Chem. Res.* **2019**, *52*, 3188−3198.
(23) McClure, D. S. Spin-Orbit Interaction in Aromatic Molecules. *J. Chem. Phys.* **1952**, *20*, 682−686.
(24) El-Sayed, M. A. The Triplet State: Its Radiative and Nonradiative Properties. *Acc. Chem. Res.* **1968**, *1*, 8−16.
(25) Lower, S. K.; El-Sayed, M. A. The Triplet State and Molecular Electronic Processes in Organic Molecules. *Chem. Rev.* **1966**, *66*, 199−241.
(26) Batchelder, L. S. Deuterium NMR in Solids. In *Encyclopedia of Nuclear Magnetic Resonance*; Wiley: New York, 2012; Vol. 2, pp 942−950.
(27) Xu, J.; Sinelnikov, R.; Huang, Y. Capturing Guest Dynamics in Metal−Organic Framework CPO-27-M (M = Mg, Zn) by ^2H Solid-State NMR Spectroscopy. *Langmuir* **2016**, *32*, 5468−5479.

https://dx.doi.org/10.1021/acs.jpcc.0c02453
J. Phys. Chem. C 2020, 124, 11625−11630